Eur. J. Mineral.
2016, **28**, 943–952
Published online 2 September 2016

Hydrogen bond system and vibrational spectroscopy of the iron sulfate fibroferrite, $Fe(OH)SO_4 \cdot 5H_2O$

GENNARO VENTRUTI[1,*], GIANCARLO DELLA VENTURA[2], FABIO BELLATRECCIA[2], MARIA LACALAMITA[1] and EMANUELA SCHINGARO[1]

[1] Dipartimento di Scienze della Terra e Geoambientali, Università di Bari, via Orabona, 4, 70125 Bari, Italy
*Corresponding author, e-mail: gennaro.ventruti@uniba.it
[2] Dipartimento Scienze, Università di Roma Tre, Largo S. Leonardo Murialdo 1, 00146 Roma, Italy

Abstract: The crystal structure of fibroferrite, $Fe(OH)SO_4 \cdot 5H_2O$, was studied by means of single-crystal X-ray diffraction and vibrational (FTIR and Raman) spectroscopies. The new diffraction data allowed to successfully locate eleven H positions and to completely define the H bond system that ensures the cohesion of the Fe-O-S chains in the fibroferrite structure. Infrared and Raman spectra are presented for the first time for this compound and commented on the basis of the crystal structure and literature data for sulfate minerals. Both FTIR and Raman spectra show, in the fundamental water stretching region, a very broad absorption extending from 3600 to 2600 cm^{-1}; peaks at 3522, 3411 and 3140 cm^{-1} can be resolved in the Raman pattern. The bands present in the low-wavenumber (<1300 cm^{-1}) region are assigned on the basis of the literature data for similar substances, and the observed multiplicity is in agreement with a symmetry reduction of the sulfate ion in the structure of fibroferrite.

Key-words: fibroferrite; iron sulfate; crystal-structure; hydrogen bond system; FTIR; Raman.

Introduction

Iron-bearing sulfates have attracted much attention in many multidisciplinary research fields (such as environmental science, catalysis, organic-bio and inorganic synthesis, electrochemistry, mineralogy and soil science). They are indeed known to be a product of the acid mine drainage (AMD) and the acid rock drainage (ARD) processes (Majzlan & Myneni, 2005; Kaksonen *et al*., 2008; Murray *et al*., 2014) as well as responsible of acid sulfate soil (ASS,Fanning, 2002; Fitzpatrick et al., 2009). For this reason, they are important indicators of environmental conditions such as pH, relative humidity, oxygen activity and sulfate activity (Nordstrom, 1982; Nordstrom & Alpers, 1999; Nordstrom *et al*., 2000; Hudson, 2003). These compounds are also largely studied as an indicator for the presence of water, and possibly biological life, on Mars (Roush, 1996; Klingelhofer *et al*., 2004; Johnson *et al*., 2007; Vicenzi *et al*., 2007; Lane *et al*., 2008).

In addition, iron sulfates are used for many technological applications and are studied for the development of novel electrode materials for lithium-ion batteries, for instance the hydroxysulfate (Gomez *et al*., 2013) and the oxysulfate (Sun *et al*., 2014), which exhibit a high iron redox potential with respect to phosphate compounds. Moreover they are currently used in many catalytic and organic–inorganic processes (Gorman *et al*., 1996). Therefore, it is of particular interest to maintain an extensive database of information about iron-bearing sulfate compounds for a wide variety of fields of interest. The use of a multimethodological approach, combining vibrational spectroscopy, in addition to X-ray diffraction (XRD), makes it possible to achieve a thorough understanding of these materials. Vibrational spectroscopies, in particular, are extremely useful having the capability to quickly identify unknown samples in different contexts, and requiring only small amounts of material, both as powders and single-crystals.

Although fibroferrite, $Fe(OH)SO_4 \cdot 5H_2O$, has been studied from a mineralogical and chemical point of view by several authors since the first half of the 20th century (Palache *et al*., 1951; Rossman, 1976; Scordari, 1981; Sabelli & Santucci, 1987), spectroscopic and structural investigations are limited. Rossman (1976) reported optical absorption and magnetic susceptibility data for all iron hydroxyl sulfate minerals with chemical compositions close to $Fe(OH)SO_4 \cdot nH_2O$, and concluded that fibroferrite had physical and structural characters quite different from the other examined members of the series. Scordari (1981) solved the crystal structure in space group $R\bar{3}$, based on a three-dimensional Patterson synthesis. He determined all non-hydrogen atoms, whereas the geometry and positions of the hydrogen bonds were only inferred. A more recent investigation (Lombardo, 2010) addressed several samples of fibroferrite of different occurrences using X-ray powder diffraction and electron microprobe techniques, concluding that cation replacements occur to very

DOI: 10.1127/ejm/2016/0028-2571
0935-1221/16/0028-2571 $ 4.50

minor extents in this compound. However no single crystals suitable for structure refinement were found (Lombardo, 2010).

The present study aims at providing a new single-crystal X-ray refinement to improve the whole structural model, including the location of hydrogen positions and the description of the hydrogen bond network. Vibrational (FTIR and Raman) data are presented for the first time for this compound, and interpreted on the basis of the improved structural model. This paper contributes to our ongoing research on hydrated sulfates (Della Ventura *et al*., 2013; Ventruti *et al*., 2015a) characterized by complex hydrogen bond systems.

Experimental procedure

The crystals investigated here were hand-picked under a binocular microscope from the same rock specimen from the dumps of the ancient lead and zinc mine of Saint Felix de Paillères (France) as studied by Scordari (1981). Fibroferrite forms as an alteration product of melanterite, as a consequence of an oxidation of Fe^{2+}, and is associated with copiapite, melanterite, pyrite, and gypsum. Fibroferrite appears as fibrous crystals forming parts of radiating aggregates, pale yellow or pale greenish gray in color with silky luster. Thin fibers of fibroferrite extend along the *c* axis, showing perfect cleavage parallel to the *c* axis. Its chemical composition is inferred to be that given by Scordari (1981), *i.e.* close to the nominal stoichiometry $Fe(OH)SO_4 \cdot 5H_2O$.

A single crystal with good diffraction behavior was selected for X-ray data collection on a Bruker AXS APEXII diffractometer with K-geometry installed at University of Bari, using monochromatized Mo*K*α-radiation and a charge-coupled device (CCD) detector, model 1K SMART. A sphere of three-dimensional data was explored by optimizing the collection strategy by the Apex program suite (Bruker, 2008) combining several ω and φ rotation sets with 0.5° frame width with 30 s acquisition time for each frame at a crystal-to-detector distance of 4 cm. Data reduction, including intensity integration, correction for Lorentz and polarization effects, was done using the software SAINT-IRIX. Empirical absorption corrections were applied to all data on the basis of the intensities of equivalent reflections by means of the multi-scan method implemented in SADABS (Blessing, 1995). Subsequent analysis of the intensity data by XPREP (Sheldrick, 2003) indicated the centrosymmetric distribution of the normalized structure factors, and reflection conditions allowed assignment of the unique space group $R\bar{3}$. The structure refinement was performed using the program CRYSTALS (Betteridge *et al*., 2003) starting from the atomic parameters of Scordari (1981). Reflections with $I > 3\sigma(I)$ were used for the structure refinement. Refined parameters were: atomic positions, anisotropic atom displacement parameters and the overall scale factor. The final stages of the refinement did not indicate the need of an extinction correction. After convergence, a difference Fourier map was calculated in order to locate the H atom positions. The structure model was implemented with eleven H atoms; O–H distances were fixed by soft constraints at 0.89(4) Å. The isotropic atom displacement parameters of hydrogen atoms were evaluated as 1.2**U*eq of the parent oxygen atom.

The crystal data, data-collection information and refinement details are listed in Table 1, atomic positions and isotropic displacement parameters are compiled in Table 2, anisotropic displacement parameters are given in Table 3, while the relevant bond length distances are provided in Table 4.

Room temperature (RT) powder FTIR spectra were collected at Università Roma Tre, on a Nicolet iS50 FTIR spectrometer equipped with a deuterated triglycine sulfate (DTGS) detector and a KBr beamsplitter. Approximately

Table 1. Refined cell parameters and data-collection parameters for the fibroferrite sample studied by single-crystal XRD.

Crystal dimensions (mm^3)	0.04 x 0.07 x 0.32
Space group	$R\bar{3}$
Unit-cell dimension *a* (Å)	24.199(3)
c (Å)	7.6476(9)
V ($Å^3$)	3878.4(8)
θ range for data collection (°)	5.0 to 31.0
Index range	$-34 \leq h,k \leq 34$
	$-10 \leq l \leq 9$
Reflections collected/independent	11639/2616
Reflections used	1136 with $I > 3\sigma(I)$
No. of refined parameters	142
Goof[a]	1.130
R_1[b] (on *F*)/ wR_2[b] (on F^2)	0.0621/0.1560
$\Delta\rho_{min}$/ $\Delta\rho_{max}$(e/$Å^3$)	−0.85/1.28

Notes: a: $[\Sigma [w(F_o^2-F_c^2)^2]/(n-p)]^{0.5}$, with *n*=number of reflections, *p*=number of parameters refined; b: $R_1=\Sigma[|F_o| - |F_c|]/\Sigma|F_o|$, $wR_2=[\Sigma[w(F_o^2-F_c^2)^2]/\Sigma[w(F_o^2)^2]]^{1/2}$.

Table 2. Atom fractional coordinates and equivalent isotropic displacement parameters ($Å^2$) in fibroferrite.

Atom	*x*	*y*	*z*	$U_{iso/equiv}$
Fe	0.34177(6)	0.39786(6)	0.71546(16)	0.0148(6)
S	0.40143(10)	0.46280(10)	0.3335(3)	0.0164(11)
O1	0.3553(3)	0.4423(3)	0.4823(7)	0.0204(4)
O2	0.3676(4)	0.4631(3)	0.1790(8)	0.0298(4)
O3	0.4559(3)	0.5251(3)	0.3643(10)	0.0285(4)
O4	0.2498(3)	0.3408(3)	0.6465(8)	0.0223(3)
O5	0.3710(3)	0.3427(3)	0.6177(7)	0.0187(4)
O6	0.3127(3)	0.4607(3)	0.7956(9)	0.0264(4)
O7	0.4321(3)	0.4634(3)	0.7836(9)	0.0273(4)
O8	0.3336(4)	0.5616(4)	0.6059(12)	0.0382(5)
O9	0.3454(4)	0.5681(4)	0.2310(13)	0.0465(5)
O10	0.2348(4)	0.4343(4)	0.3747(11)	0.0432(5)
H5	0.371(5)	0.318(4)	0.704(10)	0.023
H61	0.272(2)	0.449(5)	0.821(14)	0.032
H62	0.320(5)	0.495(4)	0.731(13)	0.032
H71	0.462(4)	0.453(5)	0.771(14)	0.034
H72	0.441(5)	0.502(3)	0.824(14)	0.034
H81	0.334(6)	0.564(6)	0.491(5)	0.046
H82	0.362(5)	0.601(3)	0.634(16)	0.046
H91	0.340(6)	0.530(3)	0.211(19)	0.055
H92	0.376(5)	0.607(3)	0.194(17)	0.055
H101	0.269(4)	0.431(6)	0.374(17)	0.050
H102	0.235(6)	0.438(6)	0.258(5)	0.050

Table 3. Anisotropic displacement parameters (Å^2) for the crystal structure of fibroferrite.

Atom	U_{11}	U_{22}	U_{33}	U_{23}	U_{13}	U_{12}
Fe	0.0156(7)	0.0146(7)	0.0127(5)	0.0001(5)	0.0017(5)	0.0066(6)
S	0.0163(11)	0.0147(11)	0.0159(10)	0.0024(8)	0.0018(8)	0.0062(9)
O1	0.031(4)	0.029(4)	0.009(3)	0.009 (3)	0.010(3)	0.021(3)
O2	0.049(5)	0.039(4)	0.011(3)	–0.001(3)	–0.004(3)	0.029(4)
O3	0.019(4)	0.019(4)	0.038(4)	–0.003(3)	0.005(3)	0.002(3)
O4	0.014(3)	0.019(3)	0.028(3)	0.003(3)	–0.003(3)	0.004(3)
O5	0.026(4)	0.024(4)	0.011(3)	–0.001(3)	0.000(3)	0.016(3)
O6	0.029(4)	0.024(4)	0.029(4)	0.005(3)	0.010(3)	0.015(3)
O7	0.010(3)	0.028(4)	0.031(4)	–0.004(3)	0.004(3)	0.000(3)
O8	0.038(5)	0.020(4)	0.053(5)	0.008(4)	0.004(4)	0.012(4)
O9	0.029(4)	0.028(4)	0.075(6)	0.009(5)	0.003(4)	0.008(4)
O10	0.021(4)	0.061(6)	0.047(5)	0.020(4)	0.003(4)	0.021(4)

Table 4. Selected interatomic distances (Å) in the crystal structure of fibroferrite.

Fe-O1	2.023(6)
Fe-O4	2.017(6)
Fe-O5*	1.956(6)
Fe-O5	1.944(6)
Fe-O6	2.062(7)
Fe-O7	2.024(6)
<Fe-O>	2.004
S-O1	1.494(6)
S-O2	1.440(7)
S-O3	1.441(7)
S-O4	1.477(7)
<S-O>	1.463

Notes: Symmetry code for equivalent position: *=2/3*y*,1/3*x*-*y*, 1/3*z*

0.5 mg of sample powder were mixed in 150 mg of KBr and pressed to a transparent pellet; spectra were collected in the range 400–4000 cm^{-1}, averaging 64 scans for both sample and background and with a 4 cm^{-1} nominal resolution. The powder spectrum at 77 K was obtained on the same pellet with a liquid-He cooled cryostat installed on a Bruker Hyperion 3000 microscope equipped with a mercury-cadmium-telluride (MCT) detector at beamline B22 (Diamond Light Source, Didcot, UK), by co-adding 128 scans for both sample and background, with 4 cm^{-1} spectral resolution. Transmission near infrared (NIR) spectra were collected on a single fiber, around 20 μm thick, using a Bruker Hyperion 3000 microscope equipped with an MCT detector connected to the Bruker Vertex V66 optical bench at INFN (Frascati, Rome), in the 7000–650 cm^{-1} range by co-adding 128 scans with 4 cm^{-1} spectral resolution at INFN (Frascati, Rome).

Single-crystal Raman spectra were collected at University of Bari using a confocal Horiba Jobin Yvon Labram HR Evolution spectrometer equipped with an Olympus optical microscope and a multichannel air-cooled CCD detector. Raman spectra were excited with the He-Ne 632.8 nm line. The laser power was decreased to ~1 mW to avoid potential local heating effects due to heavy light absorption. After the analysis, the sample was carefully inspected optically for any laser damage, and none was observed. The wavenumber accuracy was ±0.5 cm^{-1}, and the spectral resolution was < 1 cm^{-1}.

Structure description

The crystal structure of fibroferrite is based on chains consisting of vertex-sharing $Fe^{3+}O_6$ octahedra and SO_4 tetrahedra, running parallel to the *c* axis (Fig. 1). The

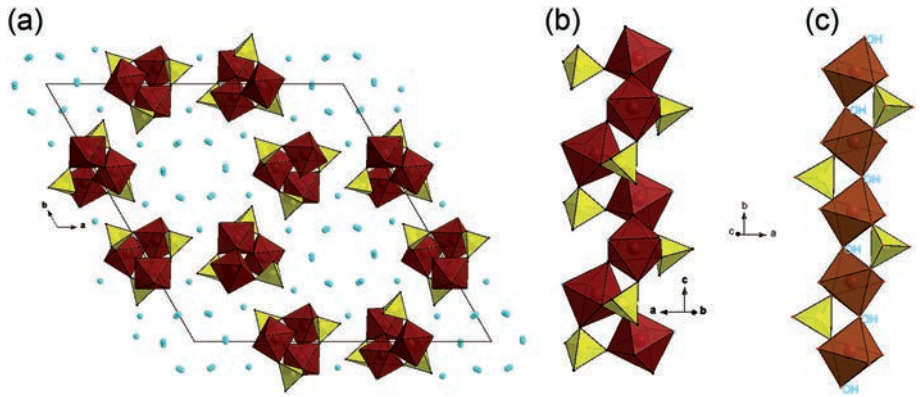

Fig. 1. (a) Structure of fibroferrite viewed along [001]. Zeolitic water groups are shown as blue spheres; (b) chains of *cis* corner-sharing octahedra decorated with SO_4 tetrahedra running along the [001] direction; (c) linear chain of Fe-octahedra linked via *trans* OH vertices in $FeOHSO_4$, parabutlerite and butlerite. (online version in colour)

Fe^{3+} coordination polyhedra are of the $[Fe^{3+}(OH)_2(H_2O)_2O_2]$ type and interlink via *cis* octahedral vertices giving rise to helical chains (Fig. 1b). The mean Fe–O distance is 2.004 Å, similar to that found in other hydrated Fe-sulfates (Scordari *et al*., 2004; Scordari & Ventruti, 2009; Ventruti *et al*., 2010; Yang *et al*., 2015). The FeO_6 octahedra are significantly distorted due to the different nature of the corners (O, OH, H_2O). The longest distances are observed for the Fe–O6 bonds to the H_2O molecules (2.024 Å), intermediate values (2.023 and 2.017 Å) involve the oxygen atoms shared with sulfur, whereas the Fe–OH bonds are the shortest (1.944 Å). The Fe^{3+}–O bond angles range from 83.9 to 97.1°.

In the structure, there is one four-fold coordinated, sulfur atom at a general position. The SO_4 tetrahedra are bidentate-bridged (Fig. 1). The non-bridging terminal S–O bonds within the tetrahedron are shorter than the bridging S–O bonds and are involved in hydrogen bonds. The average S–O distances, 1.463(7) Å, fall in the range found in most hydrated sulfates (Palmer *et al*., 1972; Hawthorne *et al*., 2000). The SO_4-tetrahedron is less distorted than the FeO_6-octahedron with $\Delta(SO_{max} - SO_{min})$ about 0.04 Å. Each sulfate tetrahedron shares two oxygen corners with $Fe^{3+}O_6$ octahedra providing further intra-chain linkages. The H_2O molecules occur both as "zeolitic" water (lying in the channels among the chains) and non-zeolitic water of FeO_6 octahedra. Adjacent chains link both directly by hydrogen bond involving the OH group and non zeolitic H_2O, and by a hydrogen-bonding network involving zeolitic water groups distributed along the channels between the Fe-S-O chains.

Although fibroferrite is chemically related to the series of basic iron sulfates characterized by the general chemical formula $Fe(OH)SO_4 \cdot nH_2O$, its structure is fundamentally different from that of other members in the series. In the iron hydroxysulfate $Fe(OH)SO_4$ (Scordari *et al*., 2004), each Fe^{3+} is bridged by *trans* hydroxyl groups to form chains of 7 Å periodicity, and these are further interconnected through sulfate groups. Also in butlerite (Fanfani *et al*., 1971) (Fig. 1c) and parabutlerite (Borene, 1970), two polymorphic modifications of the same compound $Fe(OH)SO_4 \cdot 2H_2O$, the Fe-S-O chains link trough *trans* octahedral vertices; the coordination around the iron atom is completed by water molecules, and the chains are not cross-linked by sulfate tetrahedra.

Hydrogen bonding network

Although the final *R*1 value was not substantially improved with respect to the previous work (Scordari, 1981) due to the single-crystal quality, the new data allowed to identify and refine all the hydrogen positions. Refined hydrogen-atom positions (Table 2) confirm that O6 and O7 oxygen atoms are indeed part of non-zeolitic water molecules linked to Fe^{3+} ions, whereas the O8, O9, and O10 oxygen atoms belong to interstitial water molecules, *i.e*. zeolitic water molecules.

Table 5. Hydrogen-bond lengths in fibroferrite.

D–H···A	D–H (Å)	H···A (Å)	D···A (Å)
O5 – H5···O2‡	0.88(4)	2.00	2.756
O6 – H61···O3†	0.89(4)	2.04	2.861
O6 – H62···O8	0.90(4)	1.77	2.663
O7 – H71···O3*	0.88(4)	2.06	2.819
O7 – H72···O10**	0.90(4)	1.73	2.605
O8 – H81···O9	0.88(4)	2.01	2.877
O8 – H82···O8†	0.88(4)	1.88	2.710
O9 – H91···O2	0.88(4)	2.05	2.874
O9 – H92···O9†	0.90(4)	1.84	2.729
O10 – H101···O1	0.88(4)	2.13	2.942
O10 – H102···O3†	0.90(4)	2.42	3.240

Notes: Symmetry code for equivalent positions:
‡=1/3-*x*+*y*, 2/3-*x*, 2/3+*z*; † =-1/3+*y*, 1/3-*x*+*y*, 1/3-*z*; * =-*x*,-*y*,-*z*; **=2/3+*x*-*y*, 1/3+*x*, 1/3-*z*.

Inspection of Table 5 shows that all H atoms are involved in hydrogen bonds, which can be considered as weak because most of the measured donor–acceptor ($O_D \ldots O_A$) distances exceed 2.70 Å. The strongest H linkages are O6-H62 … O8 and O7-H72 … O10, the weakest are O10-H101 … O1 and O10-H102 … O3. The oxygen atoms O5, O9 and O10 form hydrogen bonds with O2, one of the two non-bridging corners of the SO_4 tetrahedra, whereas O6 and O7 form one hydrogen bond with the remaining corner of the tetrahedron, *i.e*., with O3 of an adjacent helical chain. The hydrogen bonds involving the interaction of the structural water molecules O6 and O7 with the zeolitic water molecules O8 and O9 contribute to further connecting adjacent helical chains in a three-dimensional framework.

Bond-valence sums were calculated using the electrostatic strength function of Brown & Altermatt (1985) and the bond-valence parameters of Breese & O'Keeffe (1991) for all the non-H atoms refined in this study. Table 6 shows that, excluding the contribution of the hydrogen atoms, the bond-valence sums for O2, O3, O5, O6 and O7 are significantly lower than the ideal value of 2 valence units (vu). When the hydrogen bond contributions are included in these calculations, on the basis of the $O_D \ldots O_A$ computed distances (Ferraris & Ivaldi, 1988), the bond valence sums closely approach the ideal values. This observation confirms that: 1) O2, O3, O5, O6 and O7 are indeed the acceptor atoms for the hydrogen bonds, where O2 and O3 are non-bridging oxygen atoms of the SO_4 tetrahedron, O5 is part of the hydroxyl group linking the Fe chains, and O6, O7 belong to the water groups coordinated by the Fe^{3+} cation; 2) the interstitial water molecules at O8, O9, and O10 act simultaneously as donors and acceptors, and thus act as bridging water groups among the chains; 3) the refined model as well as the locations of the hydrogen atoms are correct. The final hydrogen-bonding scheme is illustrated in Fig. 2.

Table 6. Bond-valence analysis for the crystal structure of fibroferrite.

	O1	O2	O3	O4	O5	O6	O7	O8	O9	O10	∑
Fe	0.489			0.498	0.587	0.441	0.488				3.109
					0.606						
S	1.421	1.644	1.639	1.487							6.191
$\sum_V$	1.910	1.644	1.639	1.985	1.193	0.441	0.488				
H5		0.160			0.840						1.000
H61			0.152			0.848					1.000
H62						0.782		0.218			1.000
H71			0.177				0.852				1.000
H72							0.769			0.231	1.000
H81								0.842	0.158		1.000
H82								0.1880.812			1.000
H91		0.150							0.850		1.000
H92									0.1980.802		1.000
H101	0.135									0.865	1.000
H102			0.078							0.922	1.000
$\sum_H$	2.045	1.954	2.046	1.985	2.033	2.071	2.109	2.060	2.008	2.018	

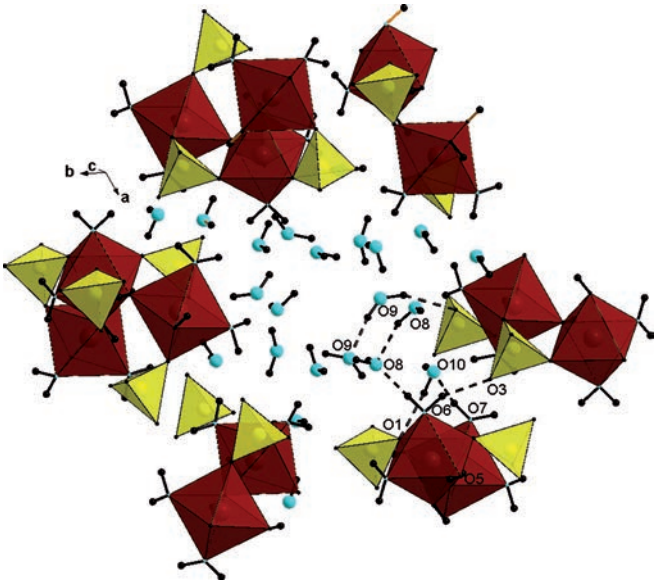

Fig. 2. Hydrogen bonding network of fibroferrite, viewed approximately along the *c* axis. (online version in colour)

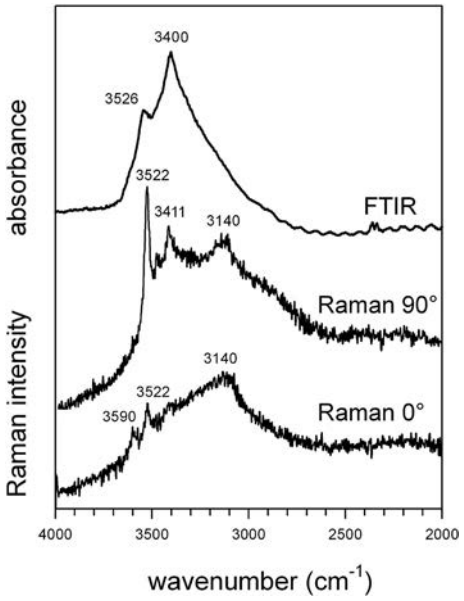

Fig. 3. Comparison of the room-temperature FTIR powder (top) and Raman spectra (down) of fibroferrite in the O-H stretching region. Raman spectra were collected on a fiber oriented parallel and perpendicular to the laser polarization.

Infrared and Raman spectroscopy

Characterization of the vibrational behavior of H_2O/OH for these highly hydrated minerals requires the combination of data from different spectral regions and different sample preparations (powder *vs* single-crystal). Figure 3 compares the powder FTIR and single-crystal Raman spectra in the O–H stretching region (4000–2000 cm^{-1}). Measured band positions are listed in Table 7, showing band assignments based on literature data for similar materials (Omori & Kerr, 1963; Adler & Kerr, 1965; Ross, 1974; Bishop *et al*., 2004; Cloutis *et al*., 2006; Lane, 2007; Della Ventura *et al*., 2013).

In the infrared pattern, a very broad and poorly resolved absorption, extending from 3600 to 2600 cm^{-1} (Fig. 3) is observed; its maximum occurs at ~3400 cm^{-1} with a second band at ~3526 cm^{-1} and two shoulders at ~3561 and ~3192 cm^{-1}. This broad feature is evidently caused by the contribution of several overlapping components, including the resonance-enhanced overtone of the H_2O bending mode ($2\nu_2$) expected around 3200 cm^{-1}. At 77 K the resolution was slightly improved (Fig. 4); at this temperature the previously described bands are well resolved (at 3546 and 3410 cm^{-1}). Several shoulders are also resolved at 3477, 3443, 3370 and 3135 cm^{-1} (Fig. 4).

Table 7 Positions (cm^{-1}) and proposed assignment for peaks observed in the RT FTIR and Raman spectra of fibroferrite.

FTIR	Raman	Assignment
5180, 4487, 4234		H_2O/OH [(υ_1, υ_3) + υ_2]
3590, 3561, 3526, 3192	3590, 3522, 3140	υ_1, υ_3 H_2O, $2\upsilon_2(H_2O)$
3400	3411	υ OH
2427, 2175		$2\upsilon_3(SO_4)$
1662, 1612		$\upsilon_2(H_2O)$
1426		Overtone(?), δ Fe-OH (?)
1221, 1134, 1081	1175, 1135, 1097, 1073	$\upsilon_3(SO_4)$ + (?)
1038, 998	1031, 998	$\upsilon_1(SO_4)$ + γ, δ Fe-OH
659, 625, 600, 508, 475	613, 590, 523, 488	$\upsilon_4(SO_4)$ + υ FeO_6
	427, 390	$\upsilon_2(SO_4)$
	297, 287, 272, 256, 219, 187, 173, 133, 114	(Fe-O,OH), lattice modes

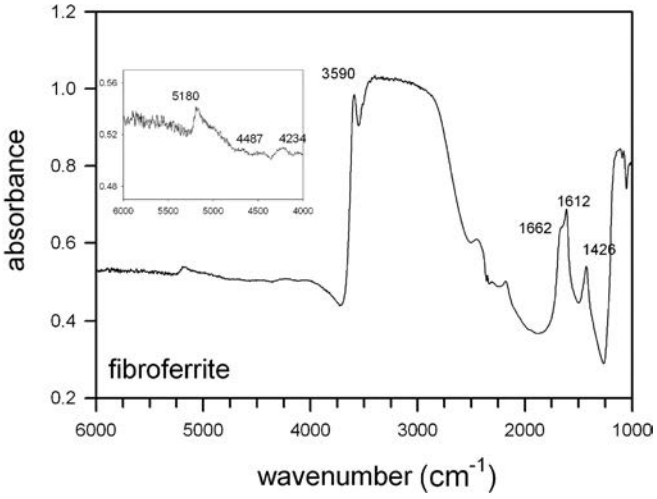

Fig. 5. FTIR spectrum of fibroferrite collected at room-temperature with unpolarized light on a single fibrous crystal. In addition the combination bands in the NIR region are magnified. Due to the sample thickness intense bands are truncated.

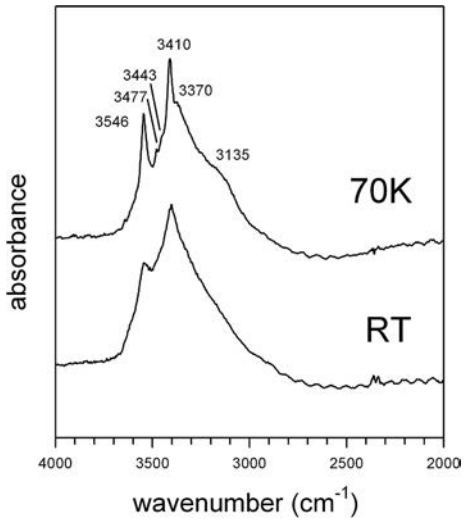

Fig. 4. FTIR powder spectra of fibroferrite collected at 77 K (top) and room temperature (down).

Two Raman spectra were collected with the fiber aligned at 0° and 90° to the polarization of the laser beam. These spectra are indeed much better resolved than the room-temperature FTIR patterns (Fig. 3) and show a very sharp peak at 3522 cm^{-1} and two well-defined absorption bands at 3411 and 3140 cm^{-1}; a weak peak is finally resolved at 3590 cm^{-1} (Fig. 3). Interestingly, the intensity of the resolved bands is extremely sensitive to the polarization direction of the beam, however we cannot draw any definitive conclusion from these spectra because, although we know that the fiber elongation coincides with the **c** crystallographic direction, it was impossible to orient the samples on the **a-b** plane for a complete polarization scheme. In the unpolarized NIR spectrum collected on a fiber (Fig. 5), the broad H_2O/OH absorption observed in the 3800–2500 cm^{-1} range collected on the KBr disk (Fig. 3) is evidently out of scale, although a well defined peak, missing in the powder pattern, is resolved at 3590 cm^{-1}. In the (ν_3 + ν_2) H_2O combination region, one broad component is present at 5180 cm^{-1} (inset in Fig. 4) with an asymmetric tail toward lower frequencies. No evident bands are observed in the 4000–4500 cm^{-1} range, where the combination (ν + δ) modes of the hydroxyl groups occur (Della Ventura *et al.*, 2013; Ventruti *et al.*, 2015a), except for two broad and poorly resolved bands at 4487 and 4234 cm^{-1}. The H_2O bending mode, which is resolved as a single broad peak centered around 1635 cm^{-1} in the powder spectrum, splits into two absorption bands at 1662 and 1612 cm^{-1} (Fig. 5). The totally symmetric ν_2 (H_2O) mode is nondegenerate, thus it is unaffected by site-group splitting; the presence of multiple $\nu_2(H_2O)$ peaks hence can be interpreted as the result of structurally distinct water molecules. Additional components resolved at 2427 and 2175 cm^{-1} are probably due to overtone modes of the sulfate group, while the 1426 cm^{-1} peak (Fig. 5) could be assigned to multiphonon modes of the Fe-OH bond (Cejka *et al.*, 2011) or to vibrational coupling between water-related peaks (Grodzicki & Piszczek, 1998).

According to the data of Table 5, in the fibroferrite structure the different O-H … O donor–acceptor bond lengths vary in the range 2.605–3.240 Å, indicative of strong to very weak hydrogen bond connections. Considering the empirical $O_D…O_A$ distance–frequency correlation of Libowitzky (1999), bands covering a broad range of frequency are thus expected, between about 3590 and 2800 cm^{-1}, and this is what we actually

observe in Fig. 3. In particular, the O10-H102….O3 distance of 3.240 Å (Table 5) corresponds to 3585 cm^{-1}, thus the relatively sharp peaks observed at this wavenumber in both the IR (Fig. 5) and Raman (Fig. 3) spectra can be assigned to one of the O–H bonds in the O10 water molecule, while the O10-H101…O1 distance of 2.942 Å (Table 5) corresponds to the sharp peak at 3522 cm^{-1} which is present in the Raman spectrum, and 3526 cm^{-1} in the FTIR spectrum (Fig. 3), that can be thus assigned to the second hydrogen bond of the same water molecule.

The spectroscopic band position of the O5-H hydroxyl group is calculated by the Libowitzky (1999) relationship at much lower wavenumbers, *i.e.* around 3350–3400 cm^{-1} based on the data of Table 5. Possibly, the sharp peak at 3411 cm^{-1} in the Raman spectrum, observed at ~3400 cm^{-1}as the most intense peak in the IR pattern (Fig. 3), could be caused by this hydroxyl group.

The powder FTIR spectrum in the low-frequency 1400–400 cm^{-1} range is displayed in Fig. 6, in comparison with the Raman spectra, collected down to 10 cm^{-1} at the same orientations as in Fig. 3. It is well known (Adler & Kerr, 1965; Ross, 1974) that a free SO_4^{2-} ion with ideal T_d symmetry has 9 degrees of freedom but only four modes of vibration: the non-degenerate symmetric stretching $\nu_1(A_1)$ at 983 cm^{-1} (Raman-active), the double degenerate symmetric in-plane bending $\nu_2(E)$ at 450 cm^{-1} (Raman-active), the triple degenerate antisymmetric stretching $\nu_3(F_2)$ at 1105 cm^{-1} and the triple degenerate out-of-plane bending $\nu_4(F_2)$ at 611 cm^{-1} (both IR- and Raman-active). In a solid sulfate structure, however, a low-symmetry S site and thus irregular arrangement of the surrounding cations may cause distortion of the SO_4 polyhedron away from the ideal T_d configuration (Adler & Kerr, 1965; Ross, 1974; Della Ventura *et al.*, 2013). As a consequence, in the IR/Raman pattern we typically observe a shift of the absorption bands to different energies, the removal of degeneracy (band splitting), and modification in the spectral activity (appearance of ideally non active IR/Raman modes). Therefore, the degree of splitting of the ν_2, ν_3 and ν_4 vibrational SO_4 peaks is related to its site symmetry and coordination geometry.

In the structure of fibroferrite one non-symmetric (C_1) SO_4^{2-} ion is present (Table 4), therefore, 3 IR + 3 Raman bands are expected as both ν_3 and ν_4 modes, whereas 2 IR + 2 Raman and 1 IR + 1 Raman bands are expected as ν_2 and ν_1 modes, respectively. Examination of Fig. 6 and Table 7 shows that the expected bands are indeed present in the spectra: in particular in the FTIR pattern, three intense bands are observed in the antisymmetric stretching region at 1221, 1134 and 1081 cm^{-1}. In the Raman spectrum, three relatively weak bands at 1175, 1135 and 1073 cm^{-1}, respectively, are observed; a fourth component at 1097 cm^{-1} is also present, whose assignment is uncertain. Two intense peaks at 1038 and 998 cm^{-1} (1031, 998 cm^{-1} in the Raman pattern, Table 7) occur in the range were ν_1 modes are expected (Adler & Kerr, 1965; Ross, 1974). The symmetric stretching mode for the (SO_4^{2-}) group is non degenerate (Adler & Kerr, 1965), thus, based on the structure refinement one peak only is expected, however there are two peaks in both the IR and the Raman spectra. Based on the literature data we thus assign one of these peaks to the Fe-OH libration, as observed in several metal sulfates (Bishop *et al.*, 2004; Cloutis *et al.*, 2006; Lane, 2007; Cejka *et al.*, 2011). The antisymmetric bending modes (ν_4) have medium intensity in both IR and Raman patterns; the band at 523 cm^{-1} in the Raman spectrum is strongly polarized (Fig. 6). The measured Raman range extends to very low wavenumbers (<100 cm^{-1}) allowing the observation of ν_2 (SO_4^{2-}), Fe-O, H_2O and lattice modes, which overlap significantly and are thus difficult to identify. Following the assignments from previous studies in the literature on sulfates (Ross, 1974; Knittle *et al.*, 2001; Murphy *et al.*, 2009; Frost *et al.*, 2013), and considering factor-group analysis considerations, the doublet at 427–390 cm^{-1} (Fig. 6) can be assigned to the ν_2 (SO_4^{2-}) mode, while bands at wavenumbers < 300 cm^{-1} could be broadly assigned to Fe-O, OH or lattice modes (Murphy *et al.*, 2009; Frost *et al.*, 2013).

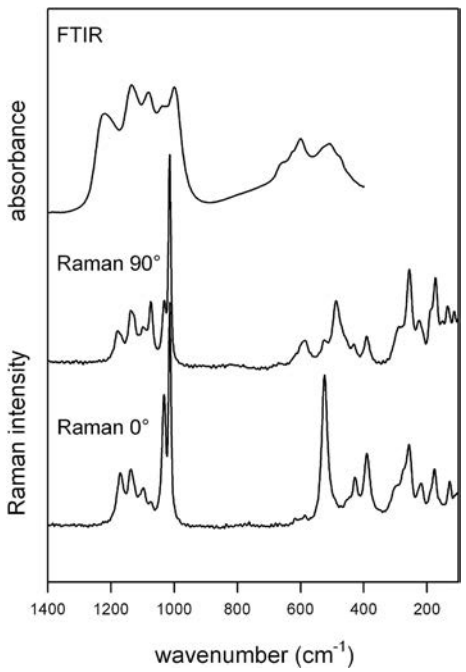

Fig. 6. The room-temperature FTIR powder spectrum (up) of fibroferrite in the low-wavenumber region compared with the Raman spectra (below) collected on a fiber oriented parallel and perpendicular to the laser polarization.

Discussion

There is a significant interest in the scientific community for Fe sulfates for several reasons, including their importance in planetary mineralogy (*e.g.* Johnson *et al.*, 2007; Lane *et al.*, 2008), in environmental

studies (Kaksonen *et al.*, 2008; Murray *et al.*, 2014) and in technology (Gomez *et al.*, 2013). This being the case, there is increasing need for new crystal-chemical data based on modern analytical techniques, and for fast and reliable methods for their identification. In this paper, we provided FTIR and Raman data not available in literature, to be used as reference data for the iron sulfate fibroferrite, $Fe(OH)SO_4 \cdot 5H_2O$. This compound in fact occurs typically as small and fibrous crystals, frequently in multiphase associations. The studied sample was fully characterized by modern single-crystal X-ray refinement, allowing to locate the hydrogen positions and describe the hydrogen-bonding scheme. The structure of fibroferrite is based on unusual helical chains of corner-sharing Fe octahedra, decorated on both sides by S tetrahedra. The reason for this chain conformation arises from the link through *cis* octahedral vertices, and it is also found in some synthetic compounds (*e.g.*, Du, 1997; Filaterov *et al.*, 2002). In these structures similar helical chains are oriented parallel to [001] and the difference in chemical composition of octahedra determines the variation in unit-cell dimensions along the chain. The butlerite, parabutlerite and $FeOHSO_4$ structures are distinguished by the octahedral linkage through *trans* octahedral vertices. The linear chain of this type has been also detected in the structure of uklonskovite (Sabelli, 1985) and a number of synthetic compounds (Gurzhii *et al.*, 2009). Fibroferrite provides the opportunity to investigate the H-bond configuration of coexisting hydroxyl group and H_2O molecules present as zeolitic, *i.e.* lying in the channels among the chains, and H_2O molecules bonded to Fe, by combining single-crystal diffraction and vibrational spectroscopy analysis. The vibrational data could thus be interpreted on the basis of this improved structural model. The presence of Raman and IR bands at significantly different frequencies reflects the different role of the H bonds in the fibroferrite structure The present work, which is part of an ongoing project on a multidisciplinary crystal-chemical study of iron-sulfates, shows that spectroscopic methods are indeed valuable tools for the study of these minerals (*e.g.* Della Ventura *et al.*, 2013; Ventruti *et al.*, 2015a), and for monitoring their transformations as a function of temperature (Ventruti *et al.*, 2013, 2015b).

Acknowledgements

The authors are grateful to Dr. Annarosa Mangone (University of Bari) for access at the Raman Laboratory funded by Potenziamento Strutturale PONa3_00369 "Laboratorio per lo Sviluppo Integrato delle Scienze e delle TEcnologie dei Materiali Avanzati e per dispositivi innovativi (SISTEMA)". We thank Diamond Light Source for access to MIRIAM beamline B22 (proposal number SM14031-1), and Dr. G. Cinque for technical assistance. The research leading to some of the results presented here has received funding from the European Community's Seventh Framework Programme (FP7/2007-2013) under the grant agreement nº 226716. E. Libowitzky (Wien) and an anonymous referee gave helpful comments that improved the manuscript.

References

Adler, H.H. & Kerr, P.F. (1965): Variations in infrared spectra, molecular symmetry and site symmetry of sulfate minerals. *Am. Mineral.*, **50**, 132–147.

Betteridge, P.W., Carruthers, J.R., Cooper, R.I., Prout, K., Watkin, D.J. (2003): Crystals version 12: Software for guided crystal structure analysis. *J. Applied Cryst.*, **36**, 1487.

Bishop, J.L., Dyar, M.D., Lane, M.D., Bandfield, J. (2004): Spectral identification of hydrated sulfates on Mars and comparison with acidic environments on Earth. *Int. J. Astrobiology*, **3**, 275–285.

Blessing, R.H. (1995): An empirical correction for absorption anisotropy. *Acta Cryst.*, **A51**, 33–38.

Borene, J. (1970): Structure cristalline de la parabutlerite. *Bull. Soc. Fr. Minéral. Cristallogr.*, **93**, 185–189.

Breese, N.E. & O'Keeffe, M. (1991): Bond-valence parameters for solids. *Acta Cryst.*, **B47**, 192–197.

Brown, I.D. & Altermatt, D. (1985): Bond valence parameters obtained from a systematic analysis of the inorganic crystal structure database. *Acta Cryst.*, **B41**, 244–247.

Bruker. (2008): APEX2, SAINT and TWINABS. Bruker AXS Inc., Madison, Wisconsin, U.S.A..

Cejka, J., Sejkora, J., Plasil, J., Bahfenne, S., Palmer, S.J., Rintoul, L., Frost, R.L. (2011): A vibrational spectroscopic study of hydrated Fe^{3+} hydroxyl-sulphates; polymorphic minerals butlerite and parabutlerite. *Spectrochim. Acta A*, **79**, 1356–1363.

Cloutis, E.A., Hawthorne, F.C., Mertzman, S.A., Krenn, K., Craig, M.A., Marcino, D., Methot, M., Strong, J., Mustard, J.F., Blaney, D.L., Bell, J.F. III, Vilas, F. (2006): Detection and discrimination of sulphate minerals using reflectance spectroscopy. *Icarus*, **184**, 121–157.

Della Ventura, G., Ventruti, G., Bellatreccia, F., Scordari, F., Cestelli-Guidi, M. (2013): FTIR transmission spectroscopy of sideronatrite, a sodium-iron hydrous sulfate. *Mineral. Mag.*, **77**, 499–507.

Du, H. (1997): PhD thesis, Jilin University, China.

Fanfani, L., Nunzi, A., Zanazzi, P.F. (1971): The crystal structure of butlerite. *Am. Mineral.*, **56**, 751–757.

Fanning, D.S. (2002): Acid sulfate soils. in "Encyclopedia of Soil Science", R. Lal, ed. Marcel Dekker, New York, 11–13.

Ferraris, G. & Ivaldi, G. (1988): Bond valence vs. bond length in O···O hydrogen bonds. *Acta Cryst.*, **B44**, 341–344.

Filaretov, A.A., Zhizhin, M.G., Komissarova, L.N., Danilov, V.P., Chernyshev, V.V., Lazoryak, B.I. (2002): Synthesis and structure of the new ammonium indium phosphate $(NH_4)In(OH)PO_4$. *J. Solid State Chem.*, **166**, 362–368.

Fitzpatrick, R.W., Shand, P., Merry, R.H. (2009): Acid Sulfate Soils. *in* "Natural history of the riverland and murraylands", J.T. Jennings, ed. Adelaide, 65–111.

Frost, R.L., López, A., Scholz, R., Xi, Y., Da Silveira, A.J., Fernandes Lima, R.M. (2013): Characterization of the sulphate mineral amarantite - $Fe^{3+}_2(SO_4)_2O \cdot 7H_2O$ using infrared, Raman spectroscopy and thermogravimetry. *Spectrochim. Acta A*, **114**, 85–91.

Gomez, M.A., Ventruti, G., Celikin, M., Assaaoudi, H., Putz, H., Becze, L., Leea, K.E., Demopoulos, G.P. (2013): The nature of synthetic basic ferric arsenate sulfate ($Fe(AsO_4)_{1-x}(SO_4)_x(OH)_x$) and basic ferric sulfate ($FeOHSO_4$): their crystallographic, molecular and electronic structure with applications in the environment and energy. *RSC Adv.*, **37**, 16840–16849.

Gorman, C.B., Bergens, S.H., Whitesides, G.M. (1996): Platinum-catalized oxidations of organic compounds by ferric sulfate - use of a redox fuel-cell to mediate complete oxidation of ethylene-glycol by dioxygen at 80°C. *J. Catal.*, **158**, 92–96.

Grodzicki, A. & Piszczek, P. (1998): A new interpretation of abnormal shift of water molecules' bending vibration frequencies in kieserite family monohydrates. *J. Mol. Struct.*, **443**, 141–147.

Gurzhii, V.V., Bessonov, A.A., Krivovichev, S.V., Tananaev, I.G., Armbruster, T., Myasoedov, B.F. (2009): Crystal chemistry of selenates with mineral-like structures: VIII. Butlerite chains in the structure of $K(UO_2)(SeO_4)(OH)(H_2O)$. *Mineral. Crystallogr.*, **51**, 833–837.

Hawthorne, F.C., Krivovichev, S.V., Burns., P.C. (2000): The crystal chemistry of sulfate minerals. in "Sulfate minerals: crystallography, geochemistry, and environmental significance", C.N. Alpers, J.L. Jambor, & B.K. Nordstrom, eds., *Rev. Mineral. Geochem*., **40**, 1–112.

Hudson, E. (2003): Sources, mineralogy, chemistry and fate of heavy metal-bearing particles in mining-affected river systems. *Mineral. Mag.*, **2**, 205–217.

Johnson, J.R., Bell, J.F., Cloutis, E., Staid, M., Farrand, W.H., McCoy, T., Rice, M., Wang, A., Yen, A. (2007): Mineralogic constraints on sulfur-rich soils from Pancam spectra at Gusev crater, Mars. *Geophys. Res. Lett.*, **34**, L13202.

Kaksonen, A.H., Dopson, M., Karnachuk, O., Tuovinen, O.H., Puhakka, J.A. (2008): Biological iron oxidation and sulfate reduction in the treatment of acid mine drainage at low temperatures. in "Psychrophiles: from biodiversity to biotechnology", R. Margesin, F. Schinner, J.C. Marx, C. Gerday, eds. Berlin, 429–454.

Klingelhöfer, G., Morris, R.V., Bernhardt, B., Schröde, C. (2004): Jarosite and hematite at meridiani planum from opportunity's mössbauer spectrometer. *Science*, **306**, 1740–1745.

Knittle, E., Phillips, W., Williams, G. (2001): An infrared and Raman spectroscopic study of gypsum at high pressure. *Phys. Chem. Minerals*, **28**, 630–640.

Lane, M.D. (2007): Mid-infrared emission spectroscopy of sulfate and sulfate-bearing minerals. *Am. Mineral.*, **92**, 1–18.

Lane, M.D., Bishop, J.L., Dyar, M.D., King, P.L., Parente, M., Hyde, B.C. (2008): Mineralogy of the paso robles soils on mars. *Am. Mineral.*, **93**, 728–739.

Libowitzky, E. (1999): Correlation of O–H stretching frequencies and O–H …O hydrogen bond lengths in minerals. *Monatsh. Chem.*, **130**, 1047–1059.

Lombardo, M. (2010): MsC. Thesis, Queens University, Ontario, Canada.

Majzlan, J. & Myneni, S.C. (2005): Speciation of iron and sulfate in acid waters: aqueous clusters to mineral precipitates. *Environ. Sci. Technol.*, **39**, 188–194.

Murphy, P.J., Smith, A.M.L., Hudson-Edwards, K.A., Dubbin, W. E., Wright, K. (2009): Raman and IR spectroscopic studies of alunite-supergroup compounds containing Al, Cr^{3+}, Fe^{3+} and V^{3+} at the B site. *Can. Mineral.*, **47**, 663–681.

Murray, J., Kirschbaum, A., Dold, B., Guimaraes, E.M., Miner, E.P. (2014): *Minerals*, **4**, 477–502.

Nordstrom, D.K. (1982): Aqueous pyrite oxidation and the consequent formation of secondary iron minerals. in "Acid Sulfate Weathering", K.A. Cedric, D.S. Fanning, I.R. Hossner, eds. Soil Science Society of America, 37–56.

Nordstrom, D.K. & Alpers, C.N. (1999): Geochemistry of acid mine waters. in "The Environmental Geochemistry of Mineral Deposits", Vol. **6A**, G.S. Plumlee & M.J. Logsdon, eds. Society of Economic Geologists, Littleton, CO, USA, 133–160.

Nordstrom, D.K., Alpers, C.N., Ptacek, C.J., Blowes, D.W. (2000): Negative pH and extremely acidic mine waters from Iron Mountain, California. *Environ. Sci. Technol.*, **34**, 254–258.

Omori, K. & Kerr, P.F. (1963): Infrared studies of saline sulphate minerals. *Geol. Soc. Am. Bull.*, **74**, 709–734.

Palache, C., Berman, H., Frondel, C. (1951): Dana's System of Mineralogy. John Wiley and Sons, Inc., New York.

Palmer, K.J., Wong, R.Y., Lee, K.S. (1972): The crystal structure of ferric ammonium sulfate trihydrate, $FeNH_4(SO_4)_2{\cdot}3H_2O$. *Acta Cryst.*, **B28**, 236–241.

Ross, S.D. (1974): Sulphates and other oxy-anions of group VI. in "The Infrared Spectra of Minerals", V.C. Farmer, ed. Mineralogical Society, London, 423–444.

Rossman, G.R. (1976): Spectroscopic characteristic and magnetic studies of ferric iron hydroxyl sulfates- the series $Fe(OH)SO_4$ and the jarosite. *Am. Mineral.*, **61**, 398–404.

Roush, T.L. (1996): Midinfrared (5.0–25 μm, 2000–4000 cm^{-1}) optical constants of hydrous carbonate, sulfate, and nitrate. *J. Geophys. Res.*, **101**, 2215–2224.

Sabelli, C. (1985): Uklonskovite, $NaMg(SO_4)F.2H_2O$: new mineralogical data and structure refinement. *Bull. Minéral.*, **108**, 133–138.

Sabelli, C. & Santucci, A. (1987): Rare sulfate minerals from the Cetine mine, Tuscany, Italy. *N. Jb. Mineral. Mh.*, **4**, 171–182.

Scordari, F. (1981): Fibroferrite: a mineral with a $\{Fe(OH)(H_2O)_2SO_4\}$ spiral chain and its relationship to $Fe(OH)SO_4$, butlerite and parabutlerite. *Tschermaks Mineral. Petrogr. Mitt.*, **28**, 17–29.

Scordari, F. & Ventruti, G. (2009): Sideronatrite, $Na_2Fe(SO_4)_2(OH){\cdot}3H_2O$: Crystal structure of the orthorhombic polytype and OD character analysis. *Am. Mineral.*, **94**, 1679–1686.

Scordari, F., Ventruti, G., Gualtieri, A.F. (2004): The structure of metahohmannite, $Fe^{3+}{}_2[O(SO_4)_2]{\cdot}4H_2O$, by in situ synchrotron powder diffraction. *Am. Mineral.*, **89**, 265–370.

Sheldrick, G.M. (2003): XPREP version 6.14. Bruker-Nonius inc, Madison, Wisconsin, USA.

Sun, M., Rousse, G., Abakumov, A.M., Van Tendeloo, G., Sougrati, M.T., Courty, M., Doublet, M.L., Tarascon, J.M. (2014): An oxysulfate $Fe_2O(SO_4)_2$ electrode for sustainable Li-based batteries. *J. Am. Chem. Soc.*, **136**, 12658−12666.

Ventruti, G., Stasi, F., Scordari, F. (2010): Metasideronatrite: crystal structure and its relation with sideronatrite. *Am. Mineral.*, **95**, 329–334.

Ventruti, G., Scordari, F., Della Ventura, G., Bellatreccia, F., Gualtieri, A.F., Lausi, A. (2013): The thermal stability of sideronatrite and its decomposition products in the system Na_2O-Fe_2O_3-SO_2-H_2O. *Phys. Chem. Minerals*, **40**, 659–670.

Ventruti, G., Della Ventura, G., Orlando, R., Scordari, F. (2015a): Structure refinement, hydrogen-bond system and vibrational spectroscopy of hohmannite, $Fe_2[(SO_4)_2O]{\cdot}8H_2O$. *Mineral. Mag.*, **79**, 11–24.

Ventruti, G., Della Ventura, G., Scordari, F., Susta, U., Gualtieri, A.F. (2015b): In-situ high-temperature XRD and FTIR investigation of hohmannite, a water-rich Fe-sulfate, and its decomposition products. *J. Therm. Anal. Calorim.*, **119**, 1793–1802.

Vicenzi, E.P., Fries, M., Fahey, A., Rost, D., Greenwood, J.P., Steele, A. (2007) Detailed elemental, mineralogical, and isotopic examination of jarosite in martian meteorite MIL 03346. 38th Lunar and Planetary Science Conference, (Lunar and Planetary Science XXXVIII), held March 12–16, 2007 in League City, Texas. LPI Contribution No. 1338, p.2335.

Yang, Z., Giester, G., Ding, K., Li, H. (2015): Crystal structure of sideronatrite-2*M*, $Na_2Fe(SO_4)_2(OH)(H_2O)_3$, a new polytype from Xitieshan lead-zinc deposit, Qinghai province, China. *Eur. J. Mineral.*, **27**, 427–432.

Received 17 March 2016
Modified version received 6 May 2016
Accepted 28 May 2016